Proceedings of the 2006 IEEE/RSJ
International Conference on Intelligent Robots and Systems
October 9 - 15, 2006, Beijing, China

Torque Modeling of Spherical Actuators with Double-layer Poles

Liang Yan, I-Ming Chen, Chee Kian Lim
*School of Mechanical &
Aerospace Engineering
Nanyang Technological University
Singapore 639798*
michen@ntu.edu.sg

Guilin Yang, Wei Lin
*Mechatronics Group
Singapore Institute of
Manufacturing Technology
Singapore 638075*
glyang@SIMTech.a-star.edu.sg

Kok-Meng Lee
*George W. Woodruff School of
Mechanical Engineering
Georgia Institute of Technology
Atlanta, Georgia, USA 30332-0405*
kokmeng.lee@me.gatech.edu

Abstract— This paper presents a design concept of spherical actuators including a ball-shaped rotor with two layers of permanent-magnet (PM) poles and a spherical-shell-like stator with two layers of circumferential air-core coils. Corresponding to the poles configuration, the torque model of the spherical actuator has been derived. The magnetic field as well as torque output have been compared with that of spherical actuator with single-layer PM-pole configuration. This generic torque modeling method can be extended for spherical actuators with multi-layer PM&coil poles which can achieve high motion resolution as well as large working range.

I. INTRODUCTION

The conventional spherical motion mechanisms are composed of several single-axis actuators, which have drawbacks of bulky structure, backlash and singularities. One promising solution is the spherical actuator which can achieve a two/three degree-of-freedom (2/3-DOF) rotational motion in only one joint. This type of actuators have the virtues of compactness, uniform motion and nonsingularity etc. Williams and Laithwaite *et al.* have done some pioneer work on the spherical induction motor [1], [2]. This induction motor can achieve 2-DOF spherical motions. Its magnetic field and torque were analyzed by Davey *et al* [3]. A 3-DOF induction spherical motor was conceptualized by Vachtsevanos *et al* [4]. Owing to the complexity in mechanical and winding design, it is difficult to produce prototype. Lee *et al.* [5] have developed a variable-reluctance spherical motor (VRSM), which has a compact size as well as a desirable working range. A nonlinear toque model which relates the current inputs and the torque output has also been presented in [6]. Permanent magnet (PM) spherical actuators which can achieve either 2-DOF motion or 3-DOF motion are developed by Wang *et al* [7], [8]. The rotor is entirely composed of magnetized rare earth materials (NdFeB). Takemura *et al.* [9], [10] designed an ultrasonic motor consisting of a bar-shaped stator and a spherical rotor. It can generate 3-DOF rotation using bending and longitudinal vibrations of the stator.

In general, electromagnetic motors offer advantages such as fast response, high torque and moderate voltage operation, etc. In addition, as an optional force/torque generating element of electromagnetic motors, PM has the virtue of no excitation losses because there is no electrical energy absorbed by the
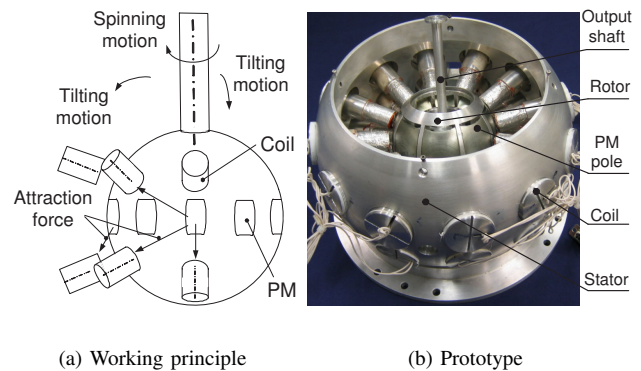

(a) Working principle   (b) Prototype

Fig. 1.   3-DOF spherical actuator with single-layer PM poles

TABLE I
STRUCTURE SPECIFICATIONS OF SPHERICAL ACTUATOR

Inner / outer stator radius	95 / 112.5 (mm)
Rotor radius	46.5 (mm)
Number of rotor poles (PM)	8 / 1 layer
Number of stator poles (coil)	24 / 2 layers
Maximum tilting angle	±11°
Maximal torque	4 (Nm)

field excitation system. For these reasons, a PM spherical actuator based on the electromagnetic principle [11], [12] is proposed in this research. One key feature of this design is that multi-layer poles can be incorporated to increase the working range and resolution of the actuator.

The working principle of this spherical actuator is illustrated in Fig. 1(a). The rare earth PMs can generate high flux density within the actuator, and the air-core coils can simplify the torque model so that the torque output has a linear relationship with the current input. With pairs of coils activated in two longitudinal directions, the rotor creates tilting motions in two orthogonal directions. By energizing the rest of the circumferential coils, the rotor can spin about its own shaft. Therefore, through varying the current inputs of coils, the actuator can produce any desirable 3-DOF rotational motion within the workspace. Based on this working principle, a

research prototype of the actuator has been developed as shown in Fig. 1(b). The specifications are listed in Table I. The large size of stator is to facilitate the magnetic field measurement inside the stator and to avoid the eddy current caused by PMs. For real products, the stator can be made of nonmetal material or laminated steel, and thus its size can be reduced by 50%. The maximum tilting angle is constrained by the coil positions.

In order to achieve high precision motion of the spherical actuator, a closed-loop control is necessary, which in turn requires an analytical torque model. A torque model for single-layer configuration of PM poles has been studied before [13]. The objective of this paper is to extend the torque modeling method to PM spherical actuators with double-layer configuration of PM poles, and to compare the torque output with that of single-layer PM-pole configuration, which helps in selecting appropriate poles pattern for actuator design. Following the same process, this torque modeling method can be applied to spherical actuators with multi-layer PM and coil poles. More layers of PM and coil poles can improve the motion resolution as well as the working range of the actuator. By adding in more layers of poles, the maximum tilting angle can be increased up to about $\pm 45°$.

II. MAGNETIC FIELD MODEL

Lorentz force law [13] is employed for the torque modeling because it is effective for force/torque computation of systems with current-carrying elements laying in the magnetic field of PMs. According to Lorentz force law, the prerequisite of torque modeling is to formulate the magnetic field of the PM-pole rotor.

A. Arrangement and Parameters of PM Pole

Two layers of PM rotor poles in alternate magnetization directions are placed around the rotor equator as shown in Fig. 2(a). There are air slots in between PM poles. And the regions on top and bottom of the rotor can also be air or low-density materials such as aluminum. These air slots generalize the study of poles arrangement. Moreover, because the density of aluminum (2.7g/cm^3) or air ($1.29 \times 10^{-3}\text{g/cm}^3$) is much lower than that of rare earth material (NdFeB 7.8g/cm^3), the inertia moment of the rotor can be reduced considerably (about 50%). This alternately magnetized poles configuration leads to the periodical variation of the magnetic field distribution circumventing the rotor. The neighboring PM poles residing in different layers are magnetized in opposite direction. Imagine a coil placed between these two PM-pole layers. One PM pole on the bottom layer creates an attraction force by interacting with the coil, whereas the other PM pole on the top layer can generate a repulsion force. Both forces cause torque in the same direction. Therefore, this poles arrangement can achieve a larger tilting torque compared with the one with same magnetization direction between two layers of PM poles.

Figure 2(b) presents the shape of a single rotor pole - an approximated dihedral cone enclosed by $ABCD$ and $abcd$. The dihedral cone can be specified by four parameters:

longitudinal angle α, latitudinal angle β, rotor radius R_r and rotor core radius R_b.

B. Region Division

In Configuration I and II, due to the material properties, the rotor space under study can be divided into three regions. Region 1 includes the volume enclosed by air space outside the rotor which is characterized by

$$\mathbf{B}_1 = \mu_0 \mathbf{H}_1, \tag{1}$$

where the subscript "1" denotes Region 1; $\mathbf{B}$ and $\mathbf{H}$ are the magnetic flux density and field intensity; and μ_0 is permeability of the free space with a value of $4\pi \times 10^{-7}\text{H/m}$. Region 2 consists all the PM rotor poles.

$$\mathbf{B}_2 = \mu_0 \mu_m \mathbf{H}_2 + \mu_0 \mathbf{M}_0, \tag{2}$$

where μ_m is the dimensionless relative recoil permeability of PM (typical value ranging between 1.05 and 1.20); $\mathbf{M}_0 = \mathbf{B}_{rem}/\mu_0$ is the residual magnetization vector in A/m; and $\mathbf{B}_{rem}$ is the remanence in T. Region 3 is the inner core made of ferromagnetic material (such as soft iron).

$$\mathbf{B}_3 = \mu_0 \mu_r \mathbf{H}_3, \tag{3}$$

where μ_r is the relative permeability of the ferromagnetic core (typically larger than 4000).

C. Residual Magnetization Vector

The PM material has the ability to attain the residual magnetization when an external magnetic field is moved. Thus it is able to create a magnetic field surrounding itself. For top PM-pole layer, the residual magnetization vector $\mathbf{M}_0$ can be represented in spherical coordinates as

$$\mathbf{M}_0 = (-1)^{p-1} \frac{\sqrt{2}}{2} |\mathbf{M}_0| \begin{bmatrix} \cos(\phi - \alpha_p)\sin\theta + \cos\theta \\ \cos(\phi - \alpha_p)\cos\theta - \sin\theta \\ -\sin(\phi - \alpha_p) \end{bmatrix}, \tag{4}$$

which is valid within the range of

$$-\frac{\alpha}{2} < \phi - \frac{\pi}{4}(p-1) < \frac{\alpha}{2}, \ \frac{\pi}{4} - \frac{\beta}{2} < \theta < \frac{\pi}{4} + \frac{\beta}{2}.$$
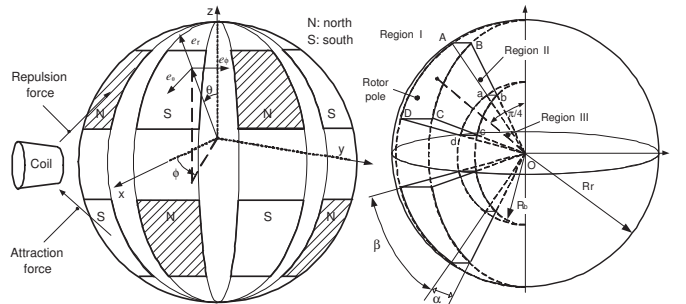

(a) Two-layer PM rotor poles   (b) Single rotor pole

Fig. 2. Arrangement of double-layer PM rotor poles

5448

For bottom PM-pole layer, $\mathbf{M}_0$ can be represented as

$$\mathbf{M}_0 = (-1)^{p-1}\frac{\sqrt{2}}{2}|\mathbf{M}_0|\begin{bmatrix}\cos(\phi-\alpha_p)\sin\theta - \cos\theta \\ \cos(\phi-\alpha_p)\cos\theta + \sin\theta \\ -\sin(\phi-\alpha_p)\end{bmatrix}, \quad (5)$$

which is valid within the range of

$$-\frac{\alpha}{2} < \phi - \frac{\pi}{4}(p-1) < \frac{\alpha}{2}, \ \frac{3\pi}{4} - \frac{\beta}{2} < \theta < \frac{3\pi}{4} + \frac{\beta}{2}.$$

Spherical harmonic expansion of M_{0r}:

In order to facilitate the solution of magnetic field subsequently, the radial component of the residual magnetization vector M_{0r} can be expressed as an expansion of spherical harmonic functions $Y_n^m(\theta,\phi)$ [14] as

$$M_{0r}^s(\theta,\phi) = \sum_{n=0}^{\infty}\sum_{m=-n}^{n}C_{n,m}Y_n^m(\theta,\phi), \quad (6)$$

where $C_{n,m}$ are coefficients determined from the surface integral of the following form:

$$C_{n,m} = \int_0^\pi \int_0^{2\pi} M_{0r}(\theta,\phi)[Y_n^{m*}(\theta,\phi)]\sin\theta d\theta d\phi, \quad (7)$$

and $Y_n^{m*}(\theta,\phi)$ denotes the complex conjugate of $Y_n^m(\theta,\phi)$. Substituting Eqns (4), (5) into Eqn. (7) gives the coefficients $C_{n,m}$. To simplify the torque formulation, only fundamental terms of $C_{n,m}$ are considered. Through computation, it is found that the fundamental terms are $n=5$, $m=\pm 4$ because all lower order terms are equal to zero. Given $\alpha = 40°$ and $\beta = 40°$. $C_{5,4} = 1.0018|\mathbf{M}_0|$ can be obtained.

D. General Solution of Magnetic Scale Potential

It can be verified that for Region i ($i = 1, 2, 3$), the scalar potentials are governed by the Laplace's equations [13]:

$$\nabla^2\Phi_i = 0, \quad (8)$$

where ∇^2 is Laplacian operator. In spherical coordinates, the general solution to the Laplace's equations characterizing Region 1, 2 and 3 has the following form

$$\Phi_i = \sum_{n=0}^{\infty}\sum_{m=-n}^{n}(\kappa_{n,i}^m r^n + \xi_{n,i}^m r^{-(n+1)})Y_n^m(\theta,\phi), \quad (9)$$

where $\kappa_{n,i}^m$ and $\xi_{n,i}^m$ are constants to be determined by the boundary conditions. From scalar potential, $\mathbf{H}_i$ can be expressed as:

$$\mathbf{H}_i = -\nabla\Phi_i. \quad (10)$$

In the spherical coordinates,

$$\begin{aligned}\mathbf{H}_i &= H_{ir}\mathbf{e}_{ir} + H_{i\theta}\mathbf{e}_\theta + H_{i\phi}\mathbf{e}_\phi \\ &= \left[-\frac{\partial\Phi_i}{\partial r}, \ -\frac{1}{r}\frac{\partial\Phi_i}{\partial\theta}, \ -\frac{1}{r\sin\theta}\frac{\partial\Phi_i}{\partial\phi}\right]^T, \end{aligned} \quad (11)$$

where $\mathbf{e}_r$, $\mathbf{e}_\theta$ and $\mathbf{e}_\phi$ are the respective unit vectors.

E. Boundary Condition

There are several boundary conditions among the three regions of the rotor space which are useful for computing the coefficients in the general solution of scalar potential.

Boundary condition at the far field: $\mathbf{B}_1|_{r\to\infty} = 0$, i.e. the magnetic flux density approaches zero when $r \to \infty$.

Finite boundary condition at $r = 0$: $\mathbf{B}_3|_{r=0} \neq \infty$, i.e. the flux density at $r = 0$ must be finite.

Continuity at the interface between two different medians:

At the air and PM surface:

$$B_{1r}|_{r=R_r} = B_{2r}|_{r=R_r}, \quad (12)$$

$$H_{1\phi}|_{r=R_r} = H_{2\phi}|_{r=R_r} \text{ and } H_{1\theta}|_{r=R_r} = H_{2\theta}|_{r=R_r}. \quad (13)$$

At the PM and soft-iron interface

$$B_{2r}|_{r=R_b} = B_{3r}|_{r=R_b}, \quad (14)$$

$$H_{2\phi}|_{r=R_b} = H_{3\phi}|_{r=R_b} \text{ and } H_{2\theta}|_{r=R_b} = H_{3\theta}|_{r=R_b}. \quad (15)$$

These conditions indicate that the flux density components normal to the interface of two neighboring media as well as the magnetic intensity components tangential to the interface must be equal.

F. Particular Solution of Magnetic Scale Potential

Solving particular solution of magnetic scale potential is to compute the coefficients $\kappa_{n,i}^m$ and $\xi_{n,i}^m$ in Eqn. (9). Following the calculating process illustrated in Fig. 3, the particular solutions of magnetic scale potential can be derived. Because only the magnetic field in Region 1 can generate torque output, attention is restricted in this region. And to simplify the computation, only fundamental terms are used. The particular solution of scalar potential is as follows.

$$\Phi_1 = \frac{945 C_{5,4} d_1}{d_2}\sqrt{\frac{11}{9!\pi}}r^{-6}\sin^4\theta\cos\theta\cos 4\phi, \quad (16)$$

where

$$d_1 = R_r^7 + \frac{11\mu_m R_b^7 R_r^{11}}{5(\mu_r-\mu_m)R_b^{11} - (5\mu_r+6\mu_m)R_r^{11}},$$

$$d_2 = 6(\mu_m - 1) + \frac{11\mu_m(5\mu_r + 6\mu_m)R_r^{11}}{5(\mu_r - \mu_m)R_b^{11} - (5\mu_r + 6\mu_m)R_r^{11}},$$

G. Magnetic Field Model

As indicted in Eqn. (10), magnetic intensity is equal to the gradient of scalar potential. Moreover, flux density is related to magnetic intensity through Eqn. (1). Therefore, the flux density can be obtained finally.

$$\begin{bmatrix}B_{1r}\\B_{1\theta}\\B_{1\phi}\end{bmatrix} = \frac{945\mu_0 C_{5,4}d_1}{d_2}\sqrt{\frac{11}{9!\pi}}r^{-7}\sin^3\theta\begin{bmatrix}6\sin\theta\cos\theta\cos 4\phi \\ (\sin^2\theta - 4\cos^2\theta)\cos 4\phi \\ 4\cos\theta\sin 4\phi\end{bmatrix}. (17)$$

It can be verified that only B_{1r} can produce torque to change the rotor orientation [13]. $B_{1\theta}$ and $B_{1\phi}$ do not produce torque on the rotor because the action lines of magnetic forces

5449

generated by $B_{1\phi}$ and $B_{1\theta}$ pass through the rotor center. As a consequence, the following discussion focuses on the radial component of the flux density B_{1r}.

III. TORQUE MODEL

By utilizing the magnetic field model, the torque generated between PM-pole rotor and coils can be formulated as follows.

A. Coil Parameters

Conical-shaped coil is utilized in this PM spherical actuator as shown in Fig. 4. The sectional area of coil can be specified by four parameters, i.e., R_0-the distance from the rotor center to the top surface of the coil, R_1-the distance from the rotor center to the bottom surface of the coil, ζ_0-the inner surface angle of the coil and ζ_1-the outer surface angle of the coil. This geometric shape can take advantage of the space surrounding the rotor effectively. It can also facilitate the
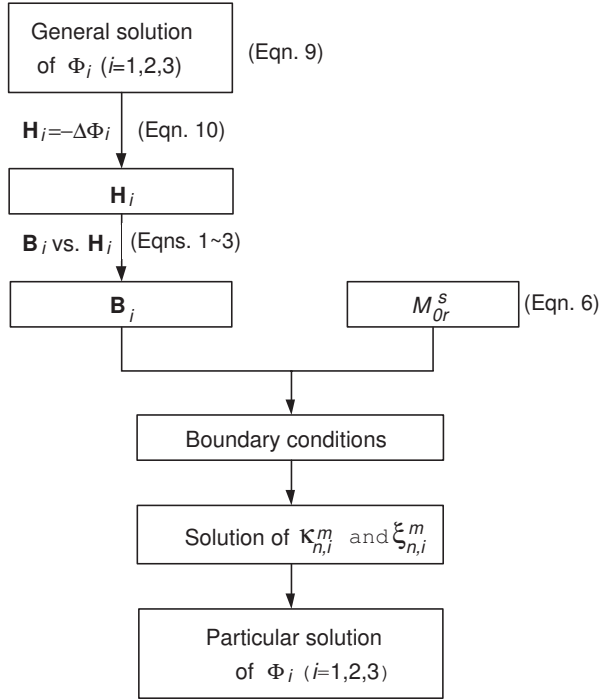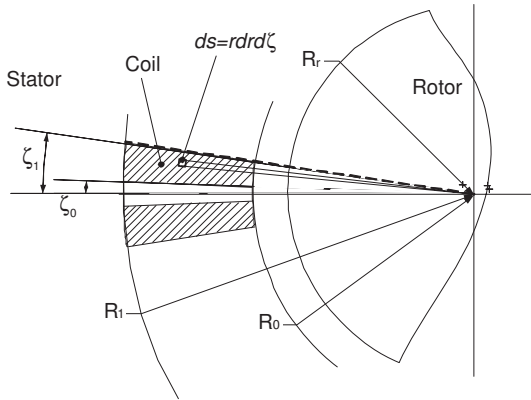

Fig. 3. Particular solution of scalar potential

Fig. 4. Sectional view of the coil shape

torque formulation in the spherical coordinates. For building prototype, off-the-shelf cylindrical-shaped coils are employed. This coil can be approximated with conical-shaped coil for similar wiring volume. Thus, the torque model can still be utilized.

B. Torque Model of Single Coil

1) Integral Formula of Torque:

Force on differential length segment of winding

Consider a differential length segment $d\mathbf{l}$ of the winding. As shown in Fig. 4, the differential sectional area of $d\mathbf{l}$ can be computed by

$$ds = rdrd\zeta. \tag{18}$$

The current passing through this section area is $J_i rdrd\zeta$, where J_i is the current density in the sectional area of the ith coil. According to Lorentz force law, the differential force on the rotor generated between the magnetic field of the PM-pole rotor and current carrying conductor $d\mathbf{l}$ is

$$
\begin{aligned}
d\mathbf{F} &= -Id\mathbf{l} \times B_{Ir}(r,\theta,\phi)\mathbf{e}_r \\
&= -J_i rdrd\zeta d\mathbf{l} \times B_{Ir}(r,\theta,\phi)\mathbf{e}_r.
\end{aligned} \tag{19}
$$

Torque on differential length segment of winding

The differential torque generated by $d\mathbf{l}$ is the multiplication of moment arm $r\mathbf{e}_r$ (the vector from rotor center to the differential winding segment) and force $d\mathbf{F}$, i.e.

$$d\mathbf{T}_i = r\mathbf{e}_r \times [-J_i rdrd\zeta d\mathbf{l} \times B_{Ir}(r,\theta,\phi)\mathbf{e}_r]. \tag{20}$$

Integral formula for single coil

Integrating the differential torque (Eqn. (20)) within the entire volume of the ith coil gives the torque occurred between this coil and the magnetic field of PM-pole rotor

$$
\begin{aligned}
\mathbf{T}_i &= \int\int\int_V r\mathbf{e}_r \times [-J_i rdrd\zeta d\mathbf{l} \times B_{Ir}(r,\theta,\phi)\mathbf{e}_r] \\
&= J_i \int_{R_0}^{R_1}\int_{\zeta_0}^{\zeta_1}\left\{\int_C r\mathbf{e}_r \times [B_{Ir}(r,\theta,\phi)\mathbf{e}_r \times d\mathbf{l}]\right\} rdrd\zeta.
\end{aligned} \tag{21}
$$

2) Solution of the torque integral formula:
Solution of torque integral formula, Eqn. (21) is to express $\mathbf{T}_i$ in terms of coil-axis position θ_i and ϕ_i in rotor frame, as well as the current input J_i, so that for any specific rotor orientation, the torque output can be determined by the current input uniquely. By substituting B_{1r} in Eqn. (17) into Eqn. (21) and taking advantage of the relation between θ_i, ϕ_i and coordinates of $d\mathbf{l}$ [13], $\mathbf{T}_i$ for one/two-layer rotor pole configurations can be obtained as follows.

$$\mathbf{T}_i = \begin{bmatrix} T_{xi} & T_{yi} & T_{zi} \end{bmatrix}^T = T_c\mathbf{f}(\theta_i,\phi_i)J_i, \tag{22}$$

5450

where

$$\mathbf{f}(\theta_i, \phi_i) = \begin{bmatrix} f_x(\theta_i, \phi_i) & f_y(\theta_i, \phi_i) & f_z(\theta_i, \phi_i) \end{bmatrix}^T$$
$$= \{ [-\sin\phi_i \ \cos\phi_i \ 0]^T (-4\sin^3\theta_i \sin^4\phi_i \cos^2\theta_i - $$
$$4\sin^3\theta_i \cos^4\phi_i \cos^2\theta_i - 6\sin^5\theta_i \cos^2\phi_i \sin^2\phi_i +$$
$$\sin^5\theta_i \sin^4\phi_i + \sin^5\theta_i \cos^4\phi_i + 24\sin^3\theta_i \cos^2\phi_i$$
$$\cos^2\theta_i \sin^2\phi_i) - [\cos\theta_i \cos\phi_i \ \cos\theta_i \sin\phi_i$$
$$-\sin\theta_i]^T (16\sin^3\theta_i \cos^3\phi_i \cos\theta_i \sin\phi_i - 16\sin^3\theta_i$$
$$\cos\phi_i \sin^3\phi_i \cos\theta_i)\},$$

$$T_c = \frac{630\mu_0 C_{5,4} d_1}{d_2} \sqrt{\frac{11\pi}{8!}} (R_0^{-3} - R_1^{-3}) G_\zeta,$$

$$G_\zeta = \frac{1}{8} G_\zeta' - \frac{3}{2} G_\zeta'' + G_\zeta''', \quad G_\zeta' = \int_{\zeta_0}^{\zeta_1} \sin^6\zeta d\zeta,$$

$$G_\zeta'' = \int_{\zeta_0}^{\zeta_1} \cos^2\zeta \sin^4\zeta d\zeta, \quad G_\zeta''' = \int_{\zeta_0}^{\zeta_1} \cos^4\zeta \sin^2\zeta d\zeta.$$

### C. Torque Model for Full Set of Coils

Corresponding to the N coils assembled in the stator, N torque equations like Eqn. (22) can be achieved. Merging them in a matrix form yields the torque model of the spherical actuator with complete set of coils

$$\mathbf{T} = T_c \begin{bmatrix} f_x(\theta_1, \phi_1) f_x(\theta_2, \phi_2) \cdots f_x(\theta_N, \phi_N) \\ f_y(\theta_1, \phi_1) f_y(\theta_2, \phi_2) \cdots f_y(\theta_N, \phi_N) \\ f_z(\theta_1, \phi_1) f_z(\theta_2, \phi_2) \cdots f_z(\theta_N, \phi_N) \end{bmatrix} \begin{bmatrix} J_1 \\ J_2 \\ \vdots \\ J_N \end{bmatrix}, \quad (23)$$

where $\begin{bmatrix} J_1 & J_2 & \cdots & J_N \end{bmatrix}^T$ is a vector of the current densities passing through Coil 1, Coil 2, $\cdots$, Coil N.

IV. COMPARISON OF TWO PM-POLE CONFIGURATIONS

The magnetic field and torque output of two PM-pole configurations, one of which includes single-layer PM poles (Configuration I) whereas the other includes double-layer PM poles (Configuration II), are compared here. The theoretical models for single-layer configuration have been derived previously. In order to facilitate the comparison, dimensions different from actual prototype is chosen for both configurations, i.e., $\alpha = 40°$ and $\beta = 40°$.
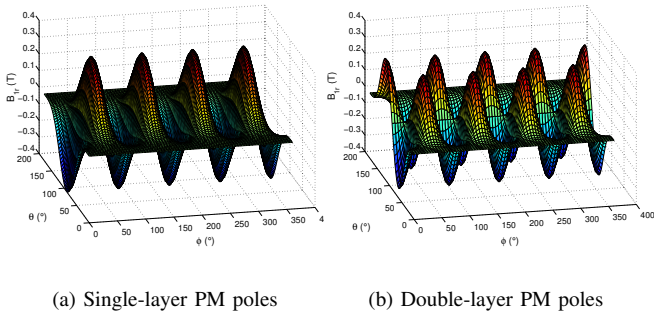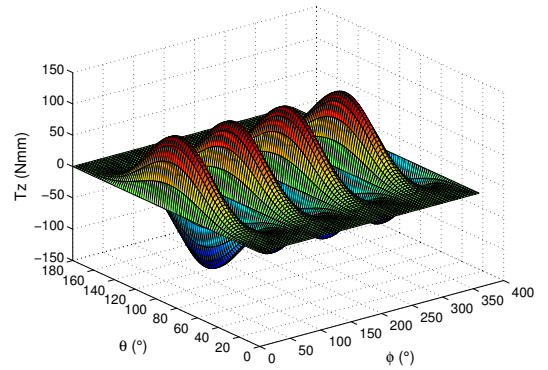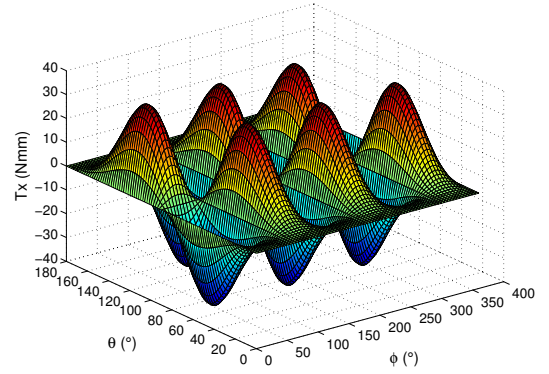

(a) Single-layer PM poles   (b) Double-layer PM poles

Fig. 5. Magnetic field distribution of PM-pole rotor ($r = 48$mm)

A. Comparison of Magnetic Field Distribution

The magnetic field can be presented visually for easy understanding. By fixing the spherical coordinate r, the radial component of flux density B_{1r} and two angular coordinates θ, ϕ form a coordinate system. The variation of B_{1r} appears as a surface in this system visually. Let $\mathbf{B}_{rem} = 1.0$T, $R_r = 46.5$mm, $R_b = 30$mm and $r = 48$mm. The magnetic field distributions for both Configuration I and Configuration II are plotted in Fig. 5. The distribution of peak values are coincident with the PM-pole arrangement. Specifically, for Configuration I, eight positive/negative peaks appears at $\theta = 90°$, which is caused by alternatively arranged PM poles along the rotor equator. It is found that the maximum value of B_{1r} for Configuration I in Fig. 5(a) (0.40T) is larger than the maximum value for Configuration II in Fig. 5(b) (0.34T). This is because the magnetized PM-pole volume for Configuration I is larger than that of Configuration II. However, for Configuration II, two positive/negative peaks appear in θ direction, which may help in increasing tilting torque of the actuator.

B. Comparison of Torque Variation

(b) Torque z

Fig. 6. Torque variation for single-layer PM poles (Configuration I)

As indicated in Eqn. (23), the total torque generated by multiple coils are the superposition of torque generated by each individual coil. Therefore, analyzing the torque generated by single coil does not lose the generality. For a spherical

5451

actuator, torque is a 3×1 vector, $\mathbf{T} = [T_x \ T_y \ T_z]^T$, where T_x, T_y and T_z are functions of θ and ϕ. Similar to the magnetic field, the variation of torque component can be visualized as a curved surface in a 3D coordinate system with respect to θ and ϕ. Given coil parameters $R_0 = 47$mm, $R_1 = 75$mm, $\zeta_0 = 2°$ and $\zeta_1 = 9°$. The number of winding turn is 800. And 3A current is supplied into the coil. The torque outputs are plotted in Fig. 6 (Configuration I) and Fig. 7 (Configuration II). Torque component in y-direction shifts $\pi/2$ in ϕ-direction from the x-component. According to these figures, it can be found that the maximum value of T_z in Configuration I (120.24Nmm) is larger than that in Configuration II (84.70Nmm), i.e. Configuration I is able to generate a high spinning torque about the rotor shaft. However, the maximum value of T_x or T_y in Configuration II (75.16Nmm) is higher than that in Configuration I (39.65Nmm), i.e. Configuration II is able to generate a high tilting torque. Therefore, the most appropriate configuration is task dependant. Additionally, it is found that the torque for both configurations can be improved four times by using the optimized coils [15].

V. CONCLUSION

This paper proposed a general design of PM spherical actuator with multiple PM and coil poles. Corresponding to the poles configurations, a generic torque modeling approach is presented. The magnetic field and torque output of the double-layer PM-pole configuration are compared with that of single-layer configuration, which shows that single-layer configuration can achieve high spinning torque whereas the double-layer configuration can realize high tilting torque. These torque models are significant for real-time motion control of the spherical actuator. Due to the parametrization of PM and coil poles in the model, design optimization of the actuators could be processed. Dynamic control and experimental analysis will be carried out in future work.

REFERENCES

[1] F. Williams, E. R. Laithwaite, and J. F. Eastham. Develpment and design of spherical induction motors. In *Proceeding of Institute of Electrical Engineers*, volume 106A, pages 471–484, December 1959.
[2] E. R. Laithwaite. Design of spherical motors. *Electrical Times (London)*, 9:921–925, June 1960.
[3] K. Davey, G. Vachtsevanos, and R. Powers. The analysis of fields and torques in spherical induction motors. *IEEE Transactions on Magnetics*, 23(1):273–282, January 1987.
[4] G. J. Vachtevanos, K. Daveyand, and K. M. Lee. Development of a novel intelligent robotic manipulator. *IEEE Control Systems Magazine*, 7(3):9–15, June 1987.
[5] K. M. Lee, R. B. Roth, and Z. Zhou. Dynamic modeling and control of a ball-joint-like variable-reluctance spherical motor. *ASME Journal of Dynamic Systems, Measurement, and Control*, 118(1):29–40, March 1996.
[6] Z. Zhou. *Real-Time Control and Characterization of a Variable Reluctance Spherical Motor*. PhD thesis, Georgia Institute of Technology, GA, USA, May 1995.
[7] J. Wang, G. W. Jewell, and D. Howe. Spherical actuators with multiple degrees-of-freedom. In *IEE Colloquium on Limited motion electrical actuation systems*, number 1998/494, pages 8/1–8/6, October 1998.
[8] J. Wang, G. W. Jewell, and D. Howe. A novel spherical actuator with three degrees-of-freedom. In *IEEE Transactions of Magnetics*, volume 34, pages 2078–2080, June 1998.
[9] K. Takemura, Y. Ohno, and T. Maeno. Design of a plate type multi-dof ultrasonic motor and its self-oscillation driving circuit. *IEEE Transactions on Mechatronics*, 9(3):474–479, September 2004.
[10] K. Takemura and T. Maeno. Design and control of an ultrasonic motor capable of generating multi-dof motion. *IEEE/ASME Transactions on Mechatronics*, 6(4):499–506, December 2001.
[11] C. K. Lim, I. M. Chen, L. Yan, G. L. Yang, W. Lin, and K. M. Lee. Design & analysis of a new variable stator pole for a dc spherical actuator. In *2005 IEEE/ASME International Conference on Advaned Intelligent Mechatronics*, pages 347–352, California, USA, July 2005.
[12] L. Yan, I. M. Chen, G. L. Yang, and K. M. Lee. Analytical and experimental investigation on the magnetic field and torque of a permanent magnet spherical actuator. *IEEE/ASME Transactions on Mechatronics*, 11(4), August 2006.
[13] L. Yan, I. M. Chen, C. K. Lim, G. L. Yang, W. Lin, and K. M. Lee. Torque modeling of a spherical actuator based on lorentz force law. In *2005 IEEE International Conference on Robotics and Automation*, pages 3657–3662, Barcelona, Spain, April 2005.
[14] J. A. R. Blais and D. A. Provins. Spherical harmonics analysis and synthesis for global multiresolution applications. *Journal of Geodesy*, 76.
[15] L. Yan, I. M. Chen, C. K. Lim, G. L. Yang, W. Lin, and K. M. Lee. Design and analysis of a permanent magnet spherical actuator. In *2005 IEEE/RSJ International Conference on Intelligent Robots and Systems*, pages 2607–2612, Alberta, Canada, August 2005.
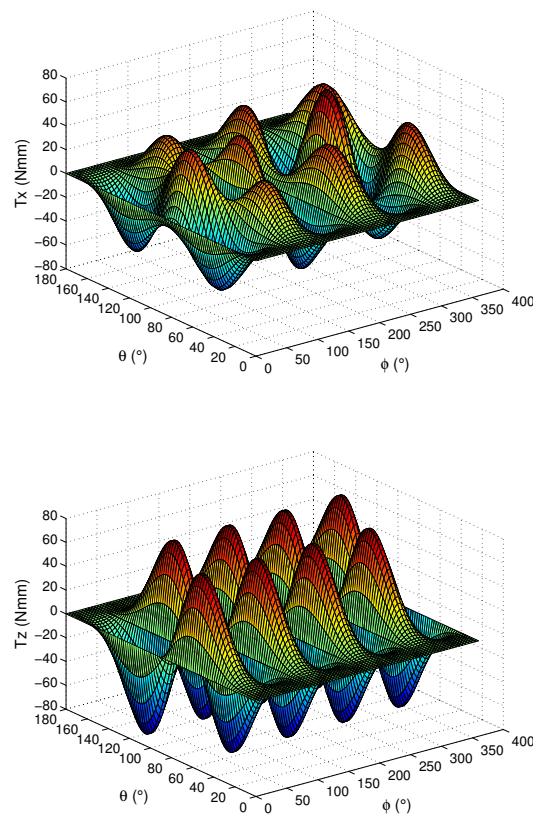
(b) Torque z

Fig. 7. Torque variation for double-layer PM poles (Configuration II)

5452